ADVANCES IN ATMOSPHERIC SCIENCES, 2021

• **Original Paper** •

The Impact of Tibetan Plateau Snow Cover on the Summer Temperature in Central Asia※

Xuke LIU, Xiaojing JIA*, Min WANG, and Qifeng QIAN

Key Laboratory of Geoscience Big Data and Deep Resource of Zhejiang Province, School of Earth Sciences, Zhejiang University, Hangzhou, Zhejiang 310027, *China*

(Received 6 January 2021; revised 21 March 2021; accepted 14 April 2021)

ABSTRACT

The current work examines the impact of the snow cover extent (SCE) of the Tibetan Plateau (TP) on the interannual variation in the summer (June–July–August) surface air temperature (SAT) over Central Asia (CA) (SAT_CA) during the 1979–2019 period. The leading mode of the summer SAT_CA features a same-sign temperature anomalies in CA and explains 62% of the total variance in SAT_CA. The atmospheric circulation associated with a warming SAT_CA is characterized by a pronounced high-pressure system dominating CA. The high-pressure system is accompanied by warm advection as well as descending motion over CA, favoring the warming of the SAT_CA. Analysis shows that the interannual variation in the summer SAT_CA is significantly positively correlated with the April SCE over the central-eastern TP. In April, higher than normal SCE over the central-eastern TP has a pronounced cooling effect on the column of the atmosphere above the TP and can persist until the following early summer. Negative and positive height anomalies appear above and to the west of the TP. In the following months, the perturbation forcing generated by the TP SCE anomalies lies near the western center of the Asian subtropical westerly jet (SWJ), which promotes atmospheric waves in the zonal direction guided by the Asian SWJ. Associated with this atmospheric wave, in the following summer, a significant high-pressure system dominates CA, which is a favorable condition for a warm summer SAT_CA.

Key words: snow cover extent, the Tibetan Plateau, Central Asia, SAT, summer

Citation: Liu, X. K., X. J. Jia, M. Wang, and Q. F. Qian, 2021: The impact of Tibetan Plateau snow cover on the summer temperature in Central Asia. *Adv. Atmos. Sci.*, https://doi.org/10.1007/s00376-021-1011-4.

Article Highlights:

- The leading mode of summer surface air temperature (SAT) in Central Asia (CA) (SAT_CA) features a same-sign pattern in CA.
- The summer SAT_CA variation was positively correlated with the changes in April snow cover extent (SCE) over the central-eastern Tibetan Plateau.
- The April SCE over the Tibetan Plateau can promote atmospheric wave patterns that contribute to summer SAT_CA.

1. Introduction

The region of Central Asia (CA) is located in the Eurasian continent and constitutes five Asian republics of the former Soviet Union, viz. Kazakhstan, Uzbekistan, Turkmenistan, Kyrgyzstan and Tajikistan (Lioubimtseva and Henebry, 2009). Far from the ocean and covered mostly by desert and gravel plains, CA is one of the largest semiarid to arid regions on Earth. It has a very fragile ecosystem and is very sensitive and vulnerable to climate change (Siegfried et al., 2012; Chen et al., 2014; Li et al., 2015; Hu et al., 2016; Yuan et al., 2017). Previous work has predicted a warming trend in CA that will be stronger than the global mean in the coming century (Giorgi, 2006; Chen et al., 2009). Within the background of global warming, extreme climate events may occur more frequently in CA, threatening climate adaptation in this area (e.g., Jiang et al., 2020). Therefore, understanding the dynamic mechanisms of climate variation over CA and improving its climate forecast skill are important.

Previous work suggests that the temperature over CA can be impacted by various factors, e.g., the location and intensity of the subtropical westerlies (e.g., Schiemann et al., 2008; Chen et al., 2019), the Pacific Decadal Oscillation (PDO) and the Siberian High (e.g., Li et al., 2012, 2020) or the polar vortex (e.g., Li et al., 2012; Yao et al.,

※ This paper is a contribution to the special issue on Third Pole Atmospheric Physics, Chemistry, and Hydrology.

* Corresponding author: Xiaojing JIA
Email: jiaxiaojing@zju.edu.cn

2015). The North Atlantic climate variability may impact the CA temperature via eastward propagating atmospheric waves along the westerly wave guide (e.g., Watanabe, 2004; Fujinami and Yasunari, 2009; Fukutomi et al., 2012; You and Jia, 2018). Lower boundary conditions, such as vegetation cover (Hiroyuki, 2004), snow cover and soil moisture (Morinaga et al., 2003; Zhao and Moore, 2006), or greenhouse gas emissions (Li et al., 2012), may also cause changes in the climate of CA. To date, most of the work exploring the factors that can be linked to the variation in the temperature in CA is mainly limited to correlation/regression analysis. The underlying potential predictors for the temperature over CA and the dynamic mechanisms are still unclear.

The Tibetan Plateau (TP) has an average elevation of over 4 km and acts as an elevated heating forcing for atmospheric variation. Changes in TP thermal conditions can contribute significantly to climate variation near the TP and downstream regions (e.g., Duan and Wu, 2005; Fujinami and Yasunari, 2009; Wu et al., 2012; Wang et al., 2018b). Recent research has revealed that the thermal condition of the TP in summer can impact climate variation in the upstream region (e.g., Lu et al., 2018; Liu et al., 2020). For example, using a numerical model, Lu et al. (2018) revealed that the summer TP heat forcing can impact the climate of upstream regions from western Asia to the North Atlantic. In winter and spring, the condition of snow is the most important thermal variable on the TP (Wang et al., 2018a, 2019; Qian et al., 2019; Jia et al., 2021). Although the process of how TP snow impacts the climate is complex, many previous studies have revealed that TP snow in the cold season has a close correlation with climate variation in East Asia and nearby regions in the following seasons. Both observational analysis and numerical model experiments illustrate that increased winter-spring snow over the TP is usually associated with weak Indian and East Asia summer monsoons; additionally, higher than average rainfall over the Yangtze valley and anomalously dry conditions in northern and southern China tend to occur in the following summer (Zhang et al., 2004; Zhao et al., 2007; Wu et al., 2012; Si and Ding, 2013; Xiao and Duan, 2016; Li et al., 2017; Wang et al., 2018a; Qian et al., 2019). Most of the previous work, however, has focused on examining the impact of TP snow on the local climate or on the downstream regions of East and South Asia, whereas few studies have examined the possible TP snow impact on the climate of CA.

The purpose of the current work is to explore whether TP snow impacts the variation in summer temperature over CA. If snow does impact the variation in summer temperature, the next question is what the dynamic mechanisms are behind this relationship. In the following, Section 2 describes the data and analysis methods that have been used in this study. Section 3 documents the characteristics of the interannual variation in the summer surface air temperature (SAT) over CA (SAT_CA) as well as its associated climate anomalies. The possible mechanism accounting for the impact of TP snow in April on SAT_CA in the following summer is investigated in section 4. The conclusions and discussions are given in section 5.

2. Data and Methods

2.1. *Data*

The original weekly Climate Data Record of Northern Hemisphere Snow Cover Extent (Robinson et al., 2012) from the Rutgers University Global Snow Lab, with a horizontal resolution of 25 km and a time span from October 1966 to the present, is available from https://climate.rutgers.edu/snowcover/docs.php?target=datareq. The snow data are produced by the Advanced Very High-Resolution Radiometer (AVHRR), the Geostationary Operational Environment Satellite System (GOES) and other visible-band satellites. Following Wang et al. (2018b), these snow cover data were converted to monthly mean data on a regular 2.5° × 2.5° latitude-longitude grid, which represents the snow cover fraction in a grid square.

The monthly mean surface air temperature data version ts4.04 from the Climate Research Unit (CRU) of the University of East Anglia (http://www.cru.uea.ac.uk/data/; Harris et al., 2014) was used in this study. The CRU data have a spatial resolution of 0.5° × 0.5° and cover the period from 1901 to 2019.

The National Centers for Environmental Prediction (NCEP)-Department of Energy (DOE) Reanalysis II (Kanamitsu et al., 2002), available from January 1979 to the present, provides monthly climatological fields obtained from the NCEP-DOE Reanalysis II (https://www.esrl.noaa.gov/psd/data/gridded/data.ncep.reanalysis2.html). Horizontal wind, air temperature, geopotential height and vertical motion (omega) at pressure levels are on regular 2.5° latitude-longitude grids. Additional variables used in this work include the air temperature at 2 m and total cloud cover, which are on T62 Gaussian grids.

In this study, we focus on the summer (June–July–August, JJA) SAT, and the dataset for the time period from 1979 to 2019 is used to perform the analysis.

2.2. *Methods*

An empirical orthogonal function (EOF) analysis was applied to the SAT_CA by constructing an area-weighted covariance matrix to obtain the leading SAT mode. This study focused on the interannual variation in the SAT_CA, and the data were filtered by a 9-year high-pass Gaussian filter to remove variations with periods longer than 10 years. A Pearson correlation and linear regression were used to capture the connection between the two variables. Student's *t*-test was applied in this study to examine the confidence level of the correlation coefficient.

The Rossby wave source (RWS) is associated with the variation in vorticity, which can be described by the following so-called forced barotropic vorticity equation (Sardeshmukh and Hoskins, 1988):

$$\left(\frac{\partial}{\partial t}+\boldsymbol{V}_{\psi}\cdot\nabla\right)\xi_{\mathrm{a}}=S\ , \tag{1}$$

$$S=-\xi_{\mathrm{a}}D-\boldsymbol{V}_{\chi}\cdot\nabla\xi_{\mathrm{a}}=-\nabla\cdot\left(\boldsymbol{V}_{\chi}\xi_{\mathrm{a}}\right)\ , \tag{2}$$

where S is the source/sink of the Rossby wave, which also represents the vorticity forcing; ξ_{a} is the absolute vorticity; D represents the divergence; $\boldsymbol{V}_{\psi}=\boldsymbol{k}\times\nabla\psi$ refers to the rotational wind velocity, and $\boldsymbol{k}$ denotes the unit vector of a Cartesian Cooidinate system; and $\boldsymbol{V}_{\chi}=\nabla\chi$ refers to the divergent wind velocity.

In this work, the total column atmospheric heat source/sink (Q1 hereafter) was calculated to examine the effect of the underlying snow cover anomalies on the above atmosphere. Following Zhao and Chen (2001), Q1 is calculated as follows:

$$\mathrm{Q1}=\mathrm{SH}+R_{\mathrm{net}}+\mathrm{LP}\ , \tag{3}$$

where SH is the sensible heat flux at the surface; R_{net} is the net radiation in the atmospheric column; and LP represents the latent heat related to condensation. When Q1 > 0, the atmospheric column is a heat source, whereas when Q1 < 0, the atmospheric column is a heat sink.

3. The Summer SAT_CA Variation and Its Associated Climate Anomalies

First, we applied EOF analysis on the summer SAT_CA (36°–55°N, 45°–90°E) for the 1979–2019 period. The leading EOF of the SAT_CA (EOF1) explained 61.8% of the summer SAT_CA and could be separated from the rest of the EOF patterns according to the criteria from North et al. (1982). The bar charts in Fig. 1b depict the normalized time series associated with EOF1 (PC1). The spatial distribution of EOF1 is shown in Fig. 1a, which is obtained by regressing the summer SAT onto PC1, and the spatial distribution over the Eurasian continent is plotted. The structure of the positive EOF1 is characterized by a same-sign warming temperature pattern dominating the central Eurasian continent. Obvious decadal variation is observed for EOF1, as seen from the low-frequency component of PC1 (black dotted line in Fig. 1b). Negative and positive values dominated PC1 before and after the mid-1990s, respectively, indicating an increasing warming of warmer temperature over CA in summer, consistent with previous work (e.g., Li et al., 2012; Yao and Chen, 2015).

As the current work focuses on the interannual variation in SAT_CA, PC1 was filtered, such that only the high-frequency component of PC1 with periods shorter than 10 years was maintained, as shown in Fig. 1c (represented by solid bars), which shows clear year-to-year variation. To better understand the representativeness of EOF1 for SAT_CA, another index was constructed by area averaging summer SAT_CA. The high-frequency component of the summer temperature index (JJA TI, and hereafter) is depicted as transparent bars in Fig. 1c. The Temporal Correlation Coefficient (TCC) between the high-frequency components of PC1 and JJA TI is 0.98, exceeding the 99% significance level, suggesting the characteristics of the SAT_CA variation is dominated by a same-sign anomalous temperature structure in CA. In the following correlation/regression analysis, JJA TI was used to represent the interannual variation in the summer SAT_CA.

The JJA TI-related climate anomalies were then obtained by regression and are presented in Fig. 2. When the summer SAT_CA is anomalously warm, significant positive height anomalies dominate the central Eurasian continent in the low (Fig. 2a) and mid-troposphere (Fig. 2b), and

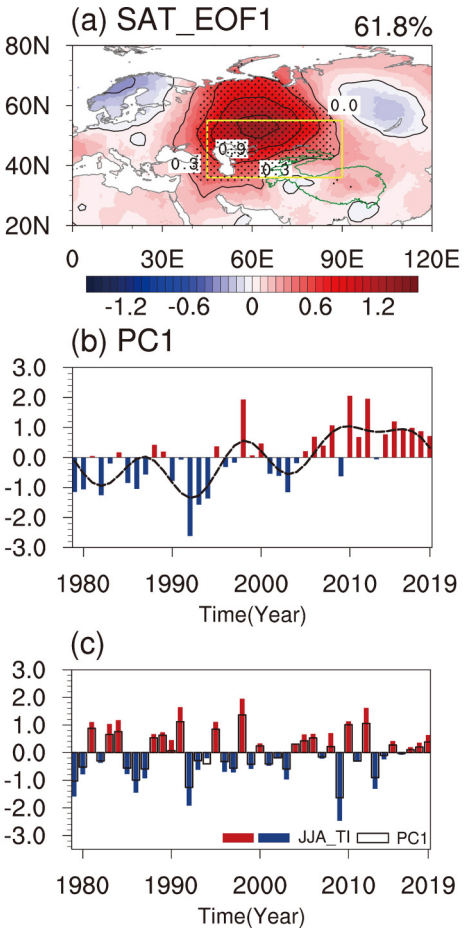

Fig. 1. (a) The spatial pattern of the first EOF (EOF1) of summer (June–July–August) surface air temperature (SAT) (°C; shading) over central Asia (36°–55°N, 45°–90°E) represented by regressing SAT onto the time series of EOF1 during the 1979–2019 period. The number in the top right corner indicates the percentage of the variance explained by EOF1. Anomalies significant at the 95% confidence level are dotted. The yellow box in Fig. 1a represents Central Asia. (b) The corresponding time series (PC1) of EOF1 (bar charts). The black dotted line represents the low-frequency component of PC1 with periods longer than 10 years. (c) High-frequency components of PC1 (represented by the solid bar charts) and the high-frequency components area-weighted averaged summer temperature index (JJA TI) over Central Asia (represented by the transparent bar charts).

also seen in the upper troposphere (not shown), suggesting an equivalent barotropic structure. To the northwest and east of these high-pressure anomalies, negative height anomalies are observed, suggesting that the atmospheric circulation anomalies associated with the variation in SAT_CA extended beyond the CA area. Associated with the high-pressure anomalies, southwesterly winds dominated mid-latitude central Eurasia between 30°–60°E, indicating enhanced warm advection from lower latitudes to CA, which could cause anomalously warm SAT in that region. At the upper level, anomalous easterly and westerly winds prevailed, which were to the south and to the north flanks of the barotropic anomalous positive geopotential height, resulting in negative and positive anomalous zonal wind speeds along 30°–50°N and 50°–70°N, respectively (Fig. 2c).

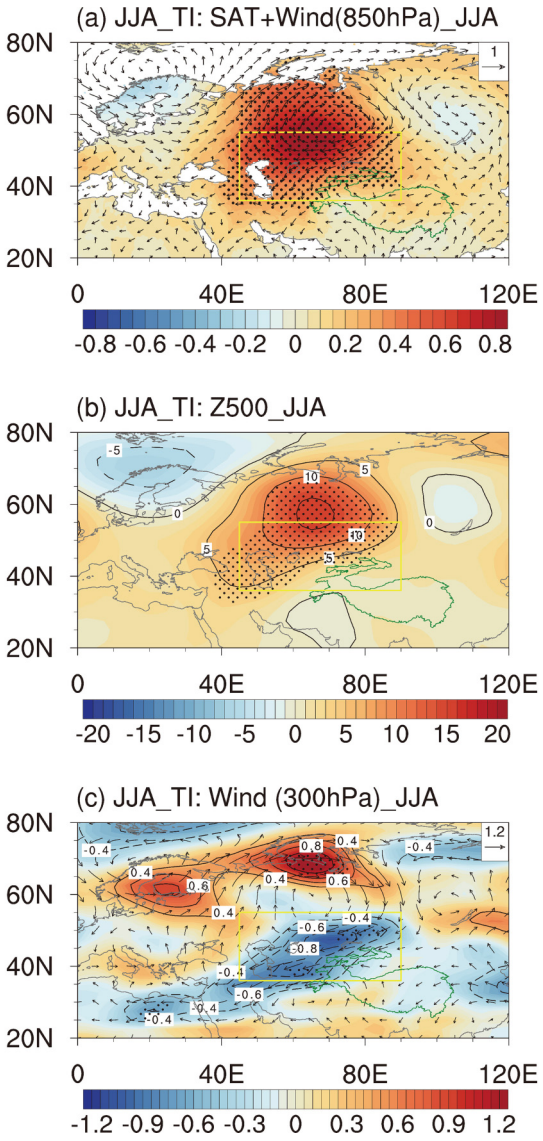

Fig. 2. Anomalies of summer (a) SAT (°C; shading) and 850-hPa wind (m s^{-1}; vectors), (b) 500-hPa geopotential height (m) and (c) 300-hPa wind (m s^{-1}; vectors) and wind speed (m s^{-1}; shading) obtained by regression against the JJA TI during the 1979-2019 period. Anomalies significant at the 95% confidence level are dotted.

Climatologically, in summer, the western center of the Asian subtropical westerly jet (SWJ) is located at approximately 40°N over the central Eurasian continent, which is to the north of the TP (Fig. 3a, contour). The vertical motion is dominated by ascent and descent airflow over the TP and CA, respectively (Fig. 3a, shading). The changes in the

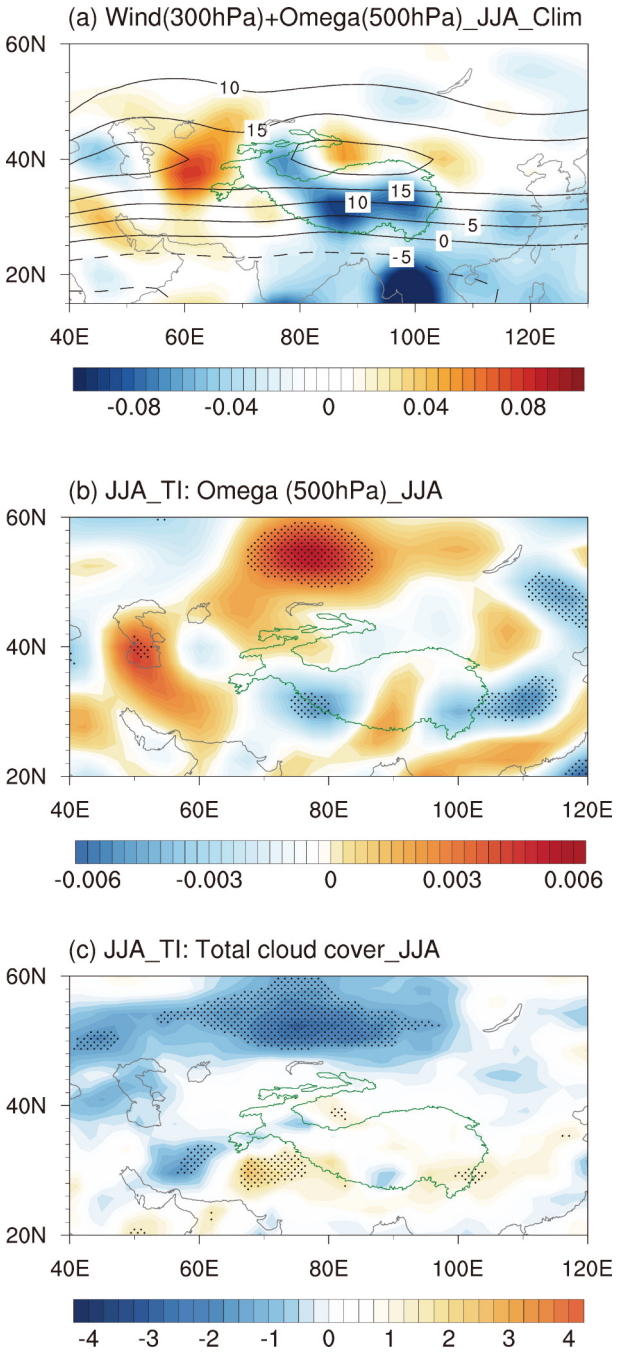

Fig. 3. (a) The climatological summer zonal wind (m s^{-1}; contour) and 500-hPa vertical velocity (Pa s^{-1}; shading). Negative and positive values of the vertical velocity denote ascent and descent motion, respectively. Anomalies of summer (b) 500-hPa vertical velocity (Pa s^{-1}; shading) and (c) total cloud cover (%; shading) obtained by regression against the JJA TI during the period of 1979–2019. Anomalies significant at the 90% confidence level are dotted.

upper-level winds associated with SAT_CA (Fig. 2c) suggest a northward shift of the Asian SWJ over the Eurasian continent. Additionally, associated with these changes is anomalous descent motion prevailing over and to the north of CA (Fig. 3b, shading), which is a favorable condition for warming the SAT over CA. The descent of the airflow over CA and the surrounding area was accompanied by a negative anomaly in total cloud cover (Fig. 3c), which means that more shortwave radiation could reach the ground and further warm the summer SAT over CA.

4. Impact of TP Snow Cover on the Variation in the Summer SAT_CA

4.1. *Possible TP Snow-SAT_CA Relationship*

To examine the possible impact of TP snow on the interannual variation in the summer SAT_CA, the Temporal Correlation Coefficient (TCC) maps of the SCE over the TP and the JJA TI from previous February to May were calculated (Fig. 4). From February to April, the TP is generally covered by positive TCCs. The most significant positive TCCs appears over the central-eastern TP in April and the TCCs are quite weak in May. This result suggests that when the April SCE over the central-eastern TP is higher than normal, in the following summer, the SAT over CA is anomalously warm. The above analysis suggests that the SCE over the TP in April might serve as a potential driver of the summer SAT_CA interannual variation.

An April Snow Index (April SI) was constructed by averaging the April SCE anomalies over the key area of the central-eastern TP (33°-39°N, 88°-105°E) (represented by the red rectangular box in Fig. 4c) to measure the changes in the April TP SCE that were closely related to the interannual variation in the summer SAT_CA. The normalized April SI is displayed in Fig. 5a by solid bar charts. The high-frequency component of the April SI is depicted as transparent bar charts in Fig. 5a and is used in the following analysis. The TCC of the April SI and JJA TI is 0.56, which is significant at the 99% confidence level. The regression of the summer SAT to April SI is presented in Fig. 5b where pronounced warming appears over CA, confirming the close relationship between the SCE over TP in the previous April and the SAT over CA in the following summer.

To further understand how the TP snow in April could be positively correlated with the summer SAT_CA, the circulation anomalies in summer associated with April SI obtained by regression are presented in Fig. 6 and Fig. 7. A comparison between Fig. 6 and Fig. 2 shows many similarities in the characteristics of the anomalous circulations. In general, when April SCE over the central-eastern TP is higher than usual, in the following summer, significant warming dominates CA (Fig. 6a, shading). Along the west flank of the positive high-pressure system, enhanced southwesterly winds penetrate CA, indicating warm advection from lower latitudes northward to the CA area (Fig. 6a, vector). Posit-

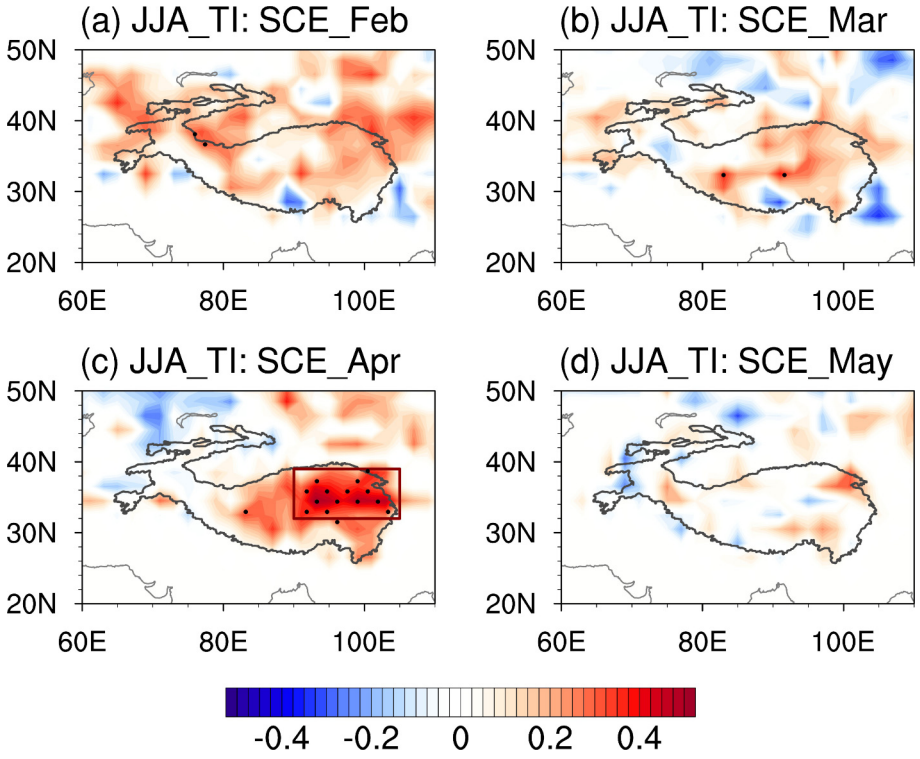

Fig. 4. Correlation maps of snow cover extent (SCE) (%; shading) for (a) February, (b) March, (c) April and (d) May against the JJA TI during the 1979–2019 period. Anomalies significant at the 95% confidence level are dotted. The red rectangle in Fig. 4c represents the key region of the central-eastern TP (32°–39°N; 89°–105°E).

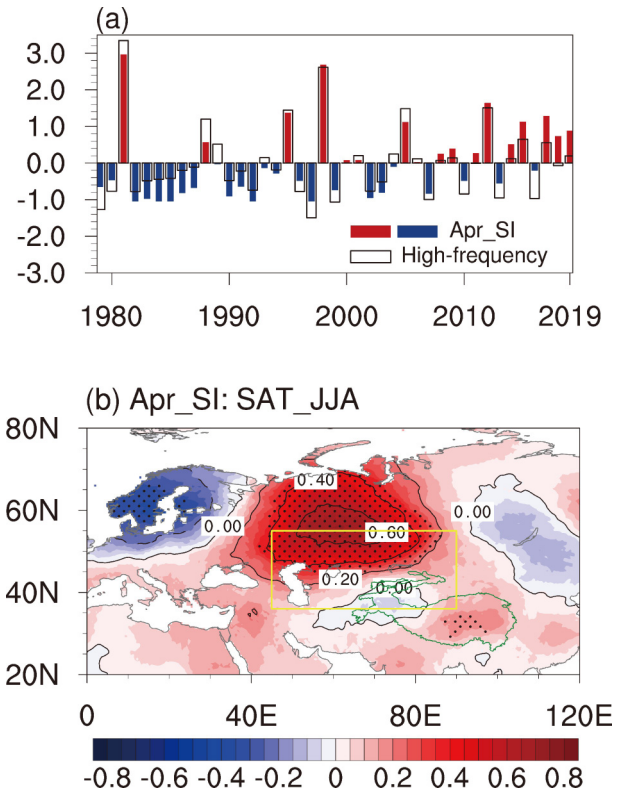

Fig. 5. (a) Transparent bar charts represent the normalized snow index (SI) obtained by the area-weighted average of snow cover extent (SCE) over the key region of the central-eastern TP (32°–39°N; 89°–105°E) (red rectangle in Fig. 4c). The solid bar charts represent the high-frequency component with periods shorter than 10 years. (b) Anomalies of summer SAT (°C) obtained by regression against the high-frequency component of the SI during the 1979–2019 period. Anomalies significant at the 95% confidence level are dotted.

ive geopotential height anomalies appear over the central Eurasian continent (Fig. 6b). Negative height anomalies can be observed over western Europe and around the Lake Baikal area (Figs. 6a, b), which together with the positive height anomalies over the central Eurasian continent form a wave train-like pattern that prevails over the whole extratropical Eurasian continent.

The spatial distribution of the anomalous summer winds associated with April SI shows significant anomalous easterly winds to the northwest of the TP, which is along the south flank of the pronounced positive geopotential height anomalies dominating CA (Fig. 6c). The changes in the winds over this region suggest a northward shift of the Asian SWJ over the central Eurasian continent. Anomalous ascent motion associated with April SI is observed to the north and west of the TP (Fig. 7a) while a negative anomaly in total cloud cover appears over central and northern CA (Fig. 7b), which is favorable for positive anomalous summer SAT_CA. The similarities of the April SI-related and JJA TI-related anomalous atmospheric circulations indicate that April TP snow may impact the interannual variation in the following summer SAT_CA by modulating atmospheric circulations.

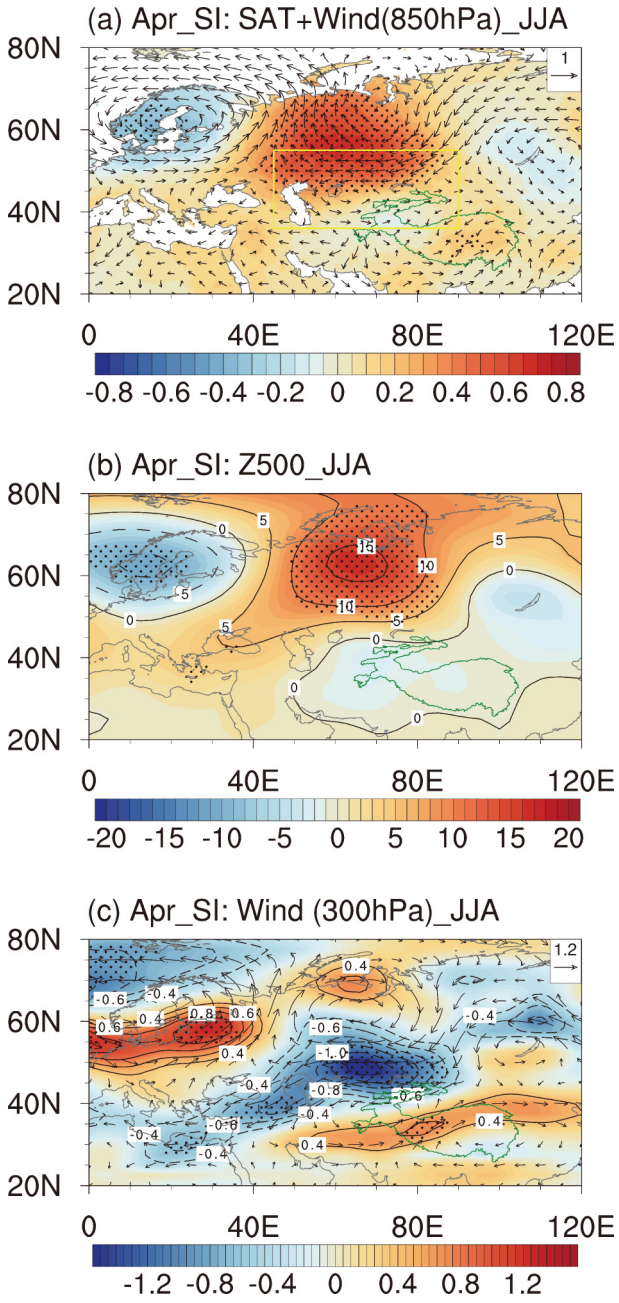

Fig. 6. Anomalies in the summer (a) SAT (°C; shading) and 850-hPa wind (m s^{-1}; vectors), (b) 500-hPa geopotential height (m) and (c) 300-hPa wind (m s^{-1}; vectors) and wind speed (m s^{-1}; shading) obtained by regression against the April SI during the period of 1979–2019. Anomalies significant at the 95% confidence level are dotted.

4.2. *Local Impact of the April TP Snow Cover Anomalies*

In the last section, we found that April TP snow is positively correlated with the interannual variation in summer SAT_CA. In this section, the possible mechanisms accounting for the April TP snow-summer SAT_CA relationship are investigated.

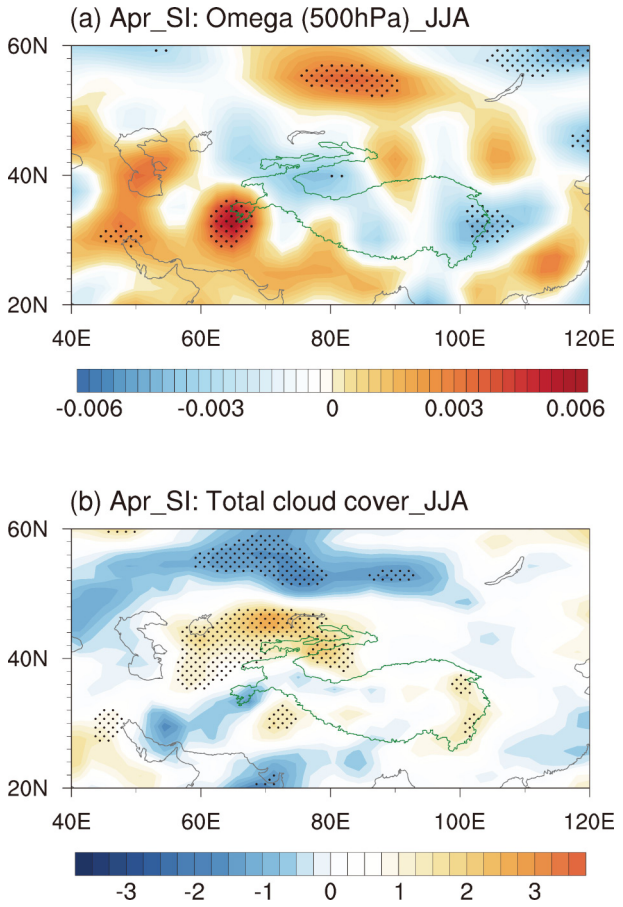

Fig. 7. Anomalies in the JJA (a) 500-hPa vertical velocity (Pa s^{-1}; shading) and (b) total cloud cover (%; shading) obtained by regression against April SI during the 1979–2019 period.

First, we examined the impact of anomalous April TP snow cover on the local climate. The April SI-related temperature and vertical motion anomalies around the TP in April are presented in Fig. 8. Compared to other underlying surface conditions, snow has much higher reflectivity for incoming shortwave radiation; thus, the albedo effect of surface snow on the overlying atmosphere can be generally described as follows: when there is excessive snow cover at the surface, due to the high snow albedo effect, more shortwave radiation is reflected back into space. Less shortwave radiation is absorbed by the ground, which could cause anomalous cooling on land. The anomalous cooling on land results in less upward sensible heat flux and causes anomalously negative air temperature. The snow effect on the atmosphere is confirmed by the results shown in Fig. 8. Associated with the positive April SI, significant negative SAT anomalies dominate the central-eastern TP (Fig. 7a). The snow-related anomalous cold air temperature can extend from the TP surface to the upper troposphere, as shown in Fig. 8b. The changes in the upper-level air temperature also suggest a weakened temperature gradient in the meridional direction over the extratropical central Eurasian continent and therefore could cause a weakened Asian SWJ (e.g., Duan et al., 2005). Associated with the positive TP snow anomalies and the column cold air temperature, the TP is dominated by negative geopotential height anomalies extending from the mid-troposphere to the upper troposphere (not shown). Climatologically, in April, the TP is dominated by ascending motion (Fig. 8c). Positive TP SCE anomalies cause cooler temperatures above the TP and weaken convection and thus anomalous descending motion dominates the TP (Fig. 8d). According to previous work (Hoskins et al., 1985; Lin and Wu, 2011; Qian et al., 2019), the upper-tropospheric cold temperature and low height anomalies introduced by excess surface snow can produce increased upper-level potential vorticity. Consequently, anomalous low-level convergence and ascending motion would follow ahead of the low pressure system, leading to increased precipitation. This is an important mechanism for maintaining surface snow. In addition, to the west and north of the TP, significantly anomalous descending motion as well as anomalously warm air temperature is observed.

4.3. *Persistent Impact of the April TP Snow Cover Anomalies*

Can the impact of the anomalous April TP SCE persist to the following summer? To answer this question, the time evolution of the TP SCE anomalies from April to May-July was calculated by regression on April SI (Fig. 9). In April, significant positive SCE anomalies appears over the east-central TP. These positive SCE anomalies decay with time but significant anomalies can still be observed in the following May and June. The results suggest that the SCE anomalies may persist into the following early summer, indicating a possible persistent forcing of snow on the above atmospheric circulations.

To further evaluate how the anomalous surface TP snow impacts the overlying atmosphere, the anomalous total heat source in the atmospheric column (Q1) in April was calculated using Eq. (3), obtained by the regression against the April SI; the results are presented in Fig. 10a. When there is greater than normal TP SCE, the TP is dominated by significant negative Q1, with the maximum values appearing over east central TP. This analysis suggests that anomalous positive TP snow has a significant cooling effect on the overlying atmosphere, consistent with previous work (e.g., Wang et al., 2019; Qian et al., 2019). Fig. 10b shows that the cooling effect of April TP SCE anomalies on the atmosphere is still significant, suggesting that the April TP snow effect can persist until the following early summer.

The calculated anomalous RWS in the upper troposphere associated with April SI in the following May–June (MJ) is presented in Fig. 11 (shading), along with climatological zonal winds at 200 hPa during this period (contours). Corresponding to a positive April SI, a negative RWS appears over the TP. Positive RWS anomalies can also be observed in the region upstream of the TP, as well as downstream of the TP, forming a wave train-like pattern prevailing on the extratropical Eurasian continent. The anomalous RWS might be caused by the anomalous height-induced upper tropospheric divergence/convergence associated with

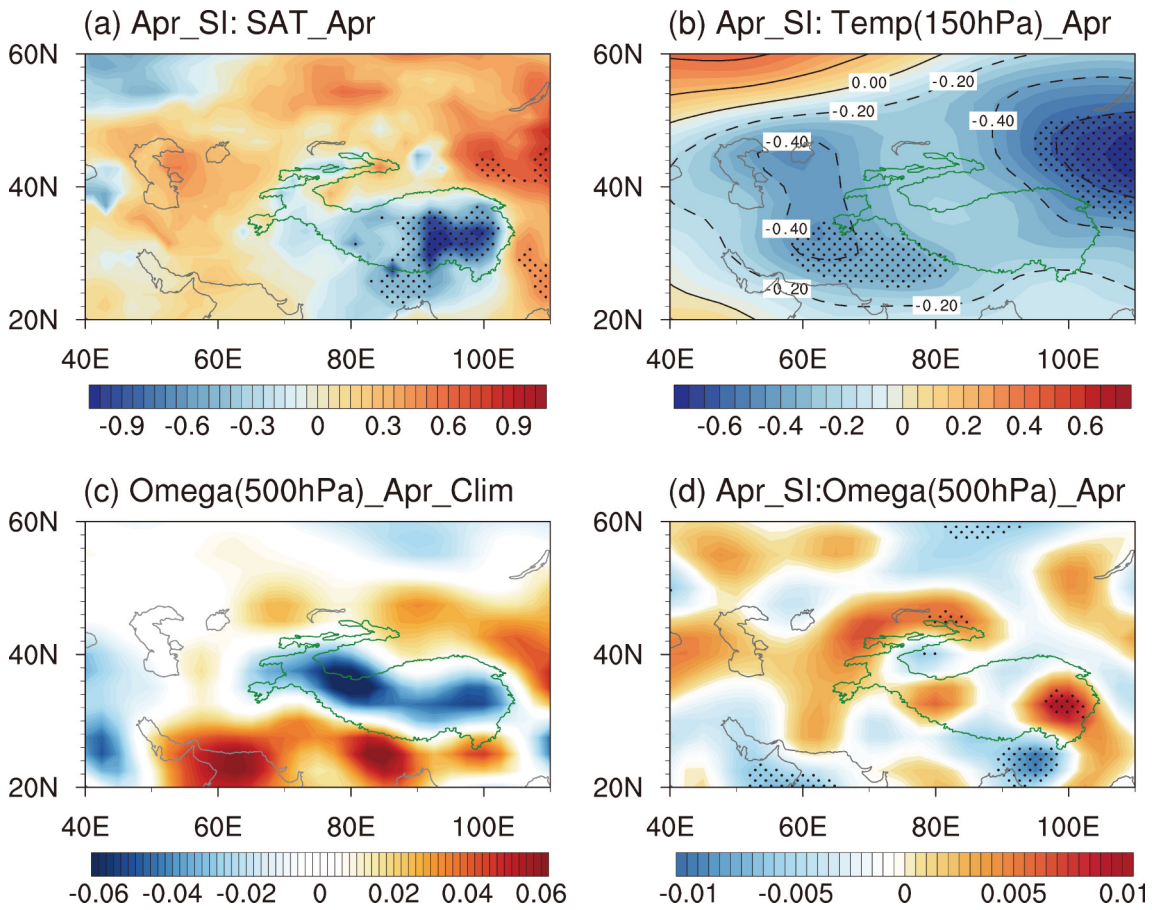

Fig. 8. Anomalies in the (a) April SAT (°C; shading). (b) April Temperature at 150 hPa (°C), (c) climatological 500-hPa vertical velocity (Pa s^{-1}; shading) and (d) 500-hPa vertical velocity (Pa s^{-1}; shading) obtained by regression against April SI during the 1979–2019 period.

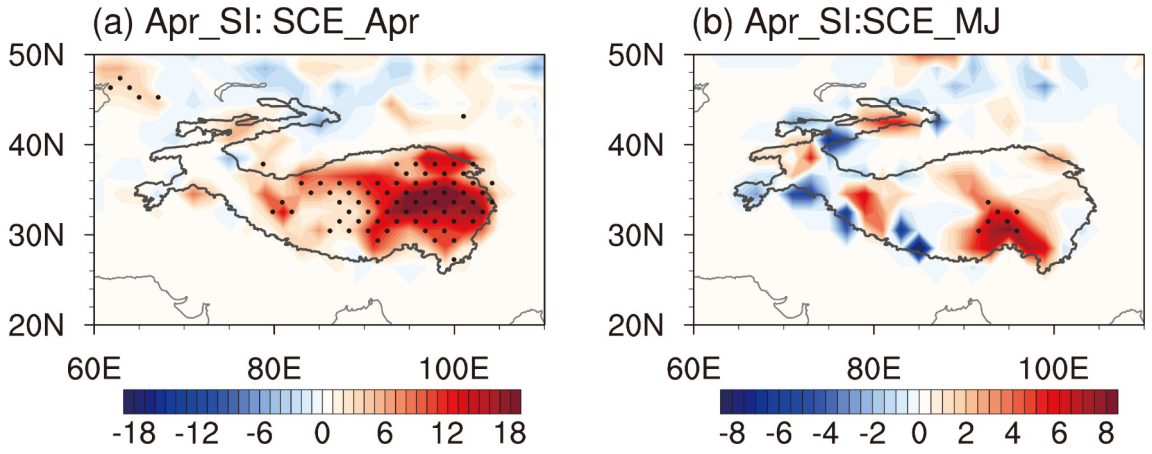

Fig. 9. Anomalies in the snow cover extent (SCE) (%; shading) for (a) April and (b) May–June obtained by regression against April SI during the 1979–2019 period. Anomalies significant at the 90% confidence level are dotted.

April SI, since as shown in Fig. 11 the anomalous April SI-related RWS is near the Asian SWJ core. As noted in previous studies, disturbances near the jet core can generate a meridionally confined atmospheric response and tend to propagate in the zonal direction with the Asian SWJ acting as a wave guide (e.g., Branstator, 2002; Li et al., 2006). The April SI-related atmospheric circulations in May–June and July–August depicted in Fig. 12 show that the wave train-like atmospheric pattern continuously develops and propagates eastward with time. A northeast-southwest tilted anomalous positive height pattern appears over the central Eurasian continent (Fig. 12b), a structure with many similarities

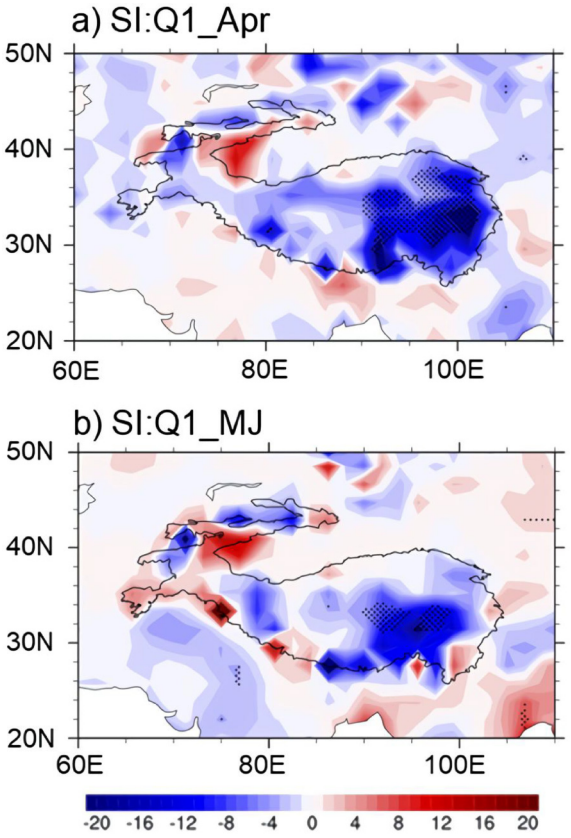

Fig. 10. Anomalies in the (a) April and (b) May–June Q1 (units: W m^{-2}) obtained by regression against the SI during the 1979–2019 period. Anomalies significant at the 95% confidence level are dotted.

to those shown in Fig. 2b over CA, favoring warming in the summer SAT_CA.

5. Conclusions and Discussion

Most previous work focused on examining the impact of TP thermal forcing on the climate of local or downstream regions of East Asia or South Asia. The current work has investigated the impact of anomalous TP snow cover on the variation in the summer SAT over CA. The focus has been given to the interannual time scale. The characteristics of the leading EOF mode of the summer SAT_CA variation features a same-sign anomalous temperature pattern in CA, and this pattern explains the dominant fraction of the summer SAT_CA variation. When the summer SAT_CA is anomalously warm, the CA is controlled by an anomalous high-pressure system, and the Asian SWJ shifts northward. Associated with these changes, pronounced warm advection prevails along the west flank of the high-pressure system, and ascending motion dominates CA, favoring a warm summer SAT_CA.

The interannual variation in the summer SAT_CA was found to be significantly positively correlated with anomalous April SCE over the central-eastern TP. When there is a greater than normal April SCE over the central-eastern TP, the SAT_CA in the following summer tends to be anomalously warm. Analysis shows that in April, the anomalous positive SCE over the central-eastern TP has a pronounced cooling effect on the atmospheric column above the TP. The summer SAT_CA-related SCE anomalies over the east central TP can persist from April to early summer. The analysis of the RWS shows that in May–June, the anomalous TP SCE-related geopotential height anomalies stimulate perturbations near the SWJ over the central Eurasian continent, easily promoting an atmospheric wave response and propagating in the zonal direction guided by the Asian SWJ. In the following summer, associated with this atmospheric wave pattern, a significant high pressure is centered over CA, which favors a warm SAT_CA in the summer.

In this work, we showed that the April TP snow and its effect can persist to early summer. In the following months, with the increase in the temperature and the decrease in snow, it is possible that the altered soil moisture over the TP, which is related to the variation in the SCE in the previous season, can help maintain the anomalous signal for a longer time. Greater details about the mechanism of the persistent effect of spring TP snow on summer need further

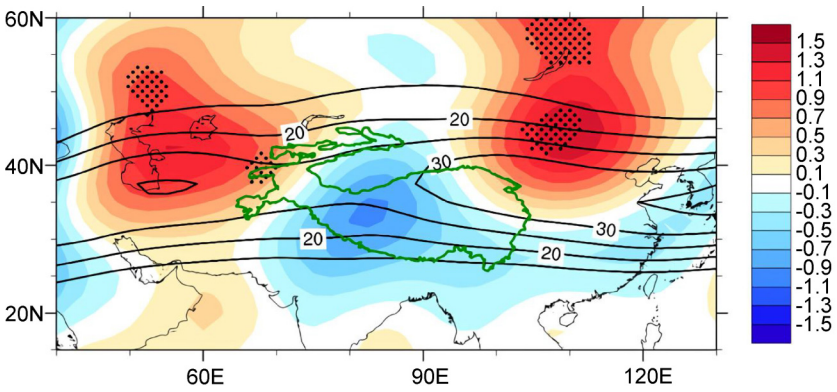

Fig. 11. Anomalies in the May–June Rossby wave source at 200 hPa obtained by regression against the SI (shading, with a scale factor of 10^{11}). The black contours refer to the climatological zonal wind (m s^{-1}). Dotted regions represent Rossby wave source anomalies significant at the 95% confidence level.

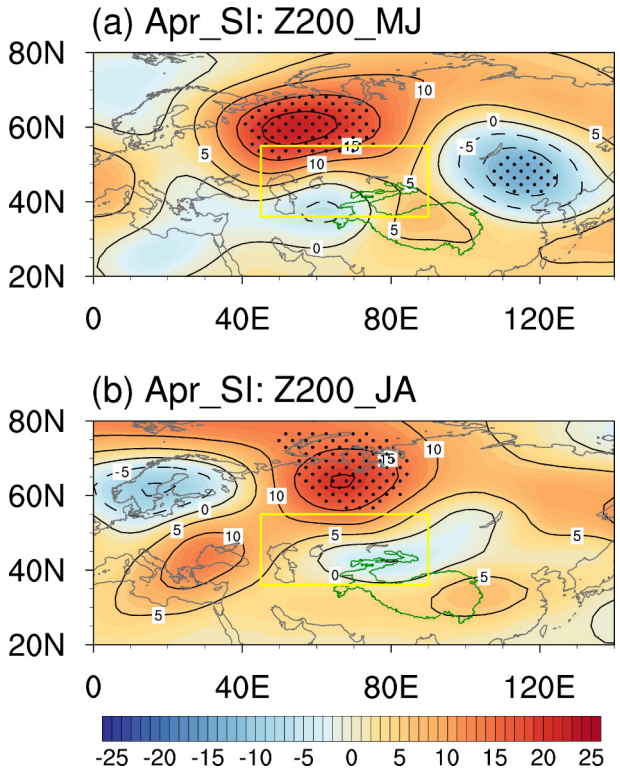

Fig. 12. Anomalies in the May–June Rossby wave source at 200 hPa obtained by regression against April SI (shading, with a scale factor of 10^{11}). The black contours refer to the climatological zonal wind (m s^{-1}). Dotted regions represent Rossby wave source anomalies significant at the 95% confidence level. The yellow box represents the central Asia (36°–55°N, 45°–90°E).

investigation. Here we focused on examining the possible impact of TP snow on the variation in the summer SAT_CA. The SST over the upstream region of the North Atlantic may also contribute to the SAT_CA variation. For example, an atmospheric wave train–like pattern originating from the North Atlantic has been reported in some previous studies to propagate eastward to East Asia (e.g., Watanabe, 2004; Li et al., 2015; Li et al., 2018; You and Jia, 2018). An atmospheric wave pattern was also observed in the current study associated with JJA TI and April SI, respectively.

It is possible that both TP snow and CA_SAT are influenced by SST in the North Atlantic. To address this possibility, we calculated the anomalous SST in the previous spring(March–April–May, MAM) associated with the JJA TI (Fig. 13a). Significant positive and negative SST anomalies can be observed over the mid-latitude and high-latitude North Atlantic, suggesting a possible impact of the North Atlantic MAM SST on the following summer CA_SAT. In contrast, the anomalous North Atlantic April SST associated with April SI (Fig. 13b) is not significant, indicating that the relationship between April TP snow and North Atlantic SST is weak. In summary, the relationship between the North Atlantic SST, the Eurasian atmospheric wave pattern, the TP snow and the summer CA_SAT can be described as follows. The North Atlantic SST in the previous MAM can impact the summer CA_SAT by exciting a Eurasian atmospheric wave pattern, as discussed in previous work (e.g., Watanabe, 2004; Li et al., 2015; You and Jia, 2018). The atmospheric wave pattern can propagate downstream to the TP area and cause anomalous TP snow (e.g.,

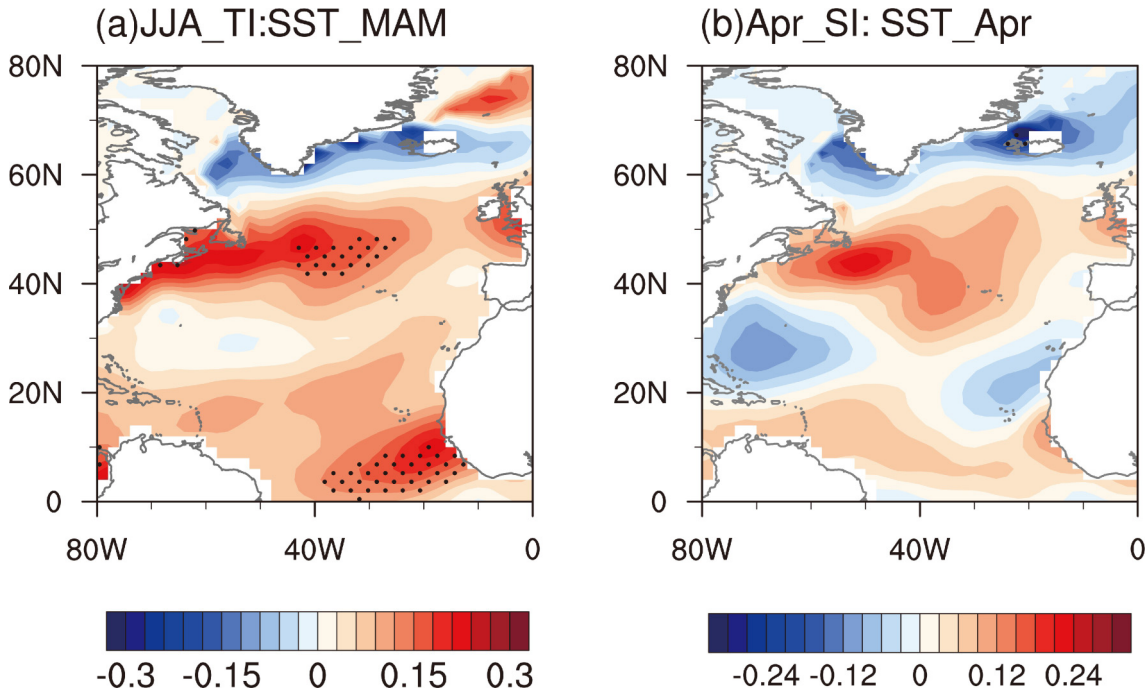

Fig. 13. (a) Anomalies in the previous March-April-May (MAM) SST (°C; shading) obtained by regression against JJA TI. (b) Anomalies in April SST (°C; shading) obtained by regression against April SI. Dotted regions represent SST anomalies significant at the 95% confidence level.

Qian et al., 2019). The TP snow anomalies then intensify the Eurasian atmospheric circulation anomalies through air-snow interactions and impact the summer CA_SAT, as revealed in the current work.

In addition to the SST, other factors, such as Arctic sea ice, may also be a factor that can impact the SAT_CA variation by modulating the westerly jet (e.g., Wu et al., 2016, He et al., 2018; Zhang et al., 2020). The relationship between the North Atlantic SST and the Arctic sea ice and the wave pattern needs further study in the future. Furthermore, it is not clear to what extent the April TP SCE can be used as a predictor to improve the seasonal forecasting accuracy of summer SAT_CA. Numerical experiments may be performed by constructing a regression model to examine this issue.

Acknowledgements. The reanalysis data are available at https://www.esrl.noaa.gov/psd/data/. The original weekly Climate Data Record of Northern Hemisphere Snow Cover Extent is available from https://climate.rutgers.edu/snowcover/docs.php?target=datareq. This research is funded by the National Natural Science Foundation of China (Grant No. 42075050).

REFERENCES

Branstator, G., 2002: Circumglobal teleconnections, the jet stream waveguide, and the North Atlantic Oscillation. *J. Climate*, **15**, 1893–1910, https://doi.org/10.1175/1520-0442(2002)015<1893:CTTJSW>2.0.CO;2.

Chen, F. H., J. S. Wang, L. Y. Jin, Q. Zhang, J. Li, and J. H. Chen, 2009: Rapid warming in mid-latitude central Asia for the past 100 years. *Frontiers of Earth Science in China*, **3**, 42–50, https://doi.org/10.1007/s11707-009-0013-9.

Chen, F. H, and Coauthors, 2019: Westerlies Asia and monsoonal Asia: Spatiotemporal differences in climate change and possible mechanisms on decadal to sub-orbital timescales. *Earth-Science Reviews*, **192**, 337–354, https://doi.org/10.1016/j.earscirev.2019.03.005.

Chen, Y. N., H. J. Deng, B. F. Li, Z. Li, and C. C. Xu, 2014: Abrupt change of temperature and precipitation extremes in the arid region of Northwest China. *Quaternary International*, **336**, 35–43, https://doi.org/10.1016/j.quaint.2013.12.057.

Duan, A. M., and G. X. Wu, 2005: Role of the Tibetan Plateau thermal forcing in the summer climate patterns over subtropical Asia. *Climate Dyn.*, **24**, 793–807, https://doi.org/10.1007/s00382-004-0488-8.

Fujinami, H., and T. Yasunari, 2009: The effects of midlatitude waves over and around the Tibetan Plateau on submonthly variability of the east Asian summer monsoon. *Mon. Wea. Rev.*, **137**, 2286–2304, https://doi.org/10.1175/2009MWR2826.1.

Fukutomi, Y., K. Masuda, and T. Yasunari, 2012: Spatiotemporal structures of the intraseasonal oscillations of precipitation over northern Eurasia during summer. *International Journal of Climatology*, **32**, 710–726, https://doi.org/10.1002/joc.2293.

Giorgi, F., 2006: Climate change hot-spots. *Geophys. Res. Lett.*, **33**, L08707, https://doi.org/10.1029/2006GL025734.

Harris, I., P. D. Jones, T. J. Osborn, and D. H. Lister, 2014: Updated high-resolution grids of monthly climatic observations-the CRU TS3. 10 Dataset. *International Journal of Climatology*, **34**, 623–642, https://doi.org/10.1002/joc.3711.

He, S. P., Y. Q. Gao, T. Furevik, H. J. Wang, and F. Li, 2018: Teleconnection between Sea Ice in the Barents Sea in June and the Silk Road, Pacific-Japan and East Asian Rainfall Patterns in August. *Adv. Atmos. Sci.*, **35**, 52–64, https://doi.org/10.1007/s00376-017-7029-y.

Hiroyuki, I., 2004: Impact of interannual variability of meteorological parameters on vegetation activity and predict possibility of vegetation activity over Mongolia. *J. Meteor. Soc. Japan*, **84**, 31–34.

Hoskins, B. J., M. E. McIntyre, and A. W. Robertson, 1985: On the use and significance of isentropic potential vorticity maps. *Q. J. R. Meteorol. Soc.*, **111**, https://doi.org/10.1002/qj.49711147002.

Hu, Z. Y., Q. X. Li, X. Chen, Z. D. Teng, C. C. Chen, G. Yin, and Y. Q. Zhang, 2016: Climate changes in temperature and precipitation extremes in an alpine grassland of Central Asia. *Theor. Appl. Climatol.*, **126**, 519–531, https://doi.org/10.1007/s00704-015-1568-x.

Jia, X. J., C. Zhang, R. G. Wu, and Q. F. Qian, 2021: Influence of Tibetan Plateau autumn snow cover on interannual variations in spring precipitation over southern China. *Climate Dyn.*, **56**, 767–782, https://doi.org/10.1007/s00382-020-05497-8.

Jiang, J., T. J. Zhou, X. L. Chen, and L. X. Zhang, 2020: Future changes in precipitation over Central Asia based on CMIP6 projections. *Environmental Research Letters*, **15**, 054009, https://doi.org/10.1088/1748-9326/ab7d03.

Kanamitsu, M., W. Ebisuzaki, J. Woollen, S. K. Yang, J. J. Hnilo, M. Fiorino, and G. L. Potter, 2002: NCEP-DOE AMIP-II reanalysis (R-2). *Bull. Amer. Meteor. Soc.*, **83**, 1631–1644, https://doi.org/10.1175/bams-83-11-1631.

Li, B. F., Y. N. Chen, and X. Shi, 2012: Why does the temperature rise faster in the arid region of northwest China? J *Geophys. Res. Atmos.*, **117**, D16115, https://doi.org/10.1029/2012JD017953.

Li, B. F., Y. P. Li, Y. N. Chen, B. H. Zhang and X. Shi, 2020: Recent fall Eurasian cooling linked to North Pacific sea surface temperatures and a strengthening Siberian high. *Nature Communications*, **11**, 5202, https://doi.org/10.1038/s41467-020-19014-2.

Li, C. F., W. Chen, X. W. Hong, and R. Y. Lu, 2017: Why was the strengthening of rainfall in summer over the Yangtze River valley in 2016 less pronounced than that in 1998 under similar preceding El Niño events?—Role of midlatitude circulation in August *Adv. Atmos. Sci.*, **34**, 1290–1300, https://doi.org/10.1007/s00376-017-7003-8.

Li, S. L., M. P. Hoerling, S. L. Peng, and K. M. Weickmann, 2006: The annular response to tropical Pacific SST forcing. *J. Climate*, **19**, 1802–1819, https://doi.org/10.1175/jcli3668.1.

Li, W. K., W. D. Guo, B. Qiu, Y. K. Xue, P.-C. Hsu, and J. F. Wei, 2018: Influence of Tibetan Plateau snow cover on East Asian atmospheric circulation at medium-range time scales. *Nature Communications*, **9**, 4243, https://doi.org/10.1038/s41467-018-06762-5.

Li, Z., Y. N. Chen, W. H. Li, H. J. Deng, and G. H. Fang, 2015: Potential impacts of climate change on vegetation dynamics in Central Asia. *J. Geophys. Res.*, **120**, 12 345–12 356, https://doi.org/10.1002/2015JD023618.

Lin, H., and Z. Wu, 2011: Contribution of the autumn Tibetan Plateau snow cover to seasonal prediction of North American winter temperature. *J. Climate*, **24**, 2801–2813, https://doi.org/10.1175/2010JCLI3889.1.

Lioubimtseva, E., and G. M. Henebry, 2009: Climate and environmental change in arid Central Asia: Impacts, vulnerability, and adaptations. *Journal of Arid Environments*, **73**, 963–977, https://doi.org/10.1016/j.jaridenv.2009.04.022.

Liu, Y. Z., Y. H. Li, J. P. Huang, Q. Z. Zhu, and S. S. Wang, 2020: Attribution of the Tibetan Plateau to northern drought. *National Science Review*, **7**, 489–492, https://doi.org/10.1093/nsr/nwz191.

Lu, M. M., S. Yang, Z. N. Li, B. He, S. He, and Z. Q. Wang, 2018: Possible effect of the Tibetan Plateau on the "upstream" climate over West Asia, North Africa, South Europe and the North Atlantic. *Climate Dyn.*, **51**, 1485–1498, https://doi.org/10.1007/s00382-017-3966-5.

Morinaga, Y., S.-F. Tian, and M. Shinoda, 2003: Winter snow anomaly and atmospheric circulation in Mongolia. *International Journal of Climatology*, **23**, 1627–1636, https://doi.org/10.1002/joc.961.

North, G. R., T. L. Bell, R. F. Cahalan, and F. J. Moeng, 1982: Sampling errors in the estimation of empirical orthogonal functions. *Mon. Wea. Rev.*, **110**, 699–706, https://doi.org/10.1175/1520-0493(1982)110<0699:seiteo>2.0.co;2.

Qian, Q. F., X. J. Jia, and R. G. Wu, 2019: Changes in the impact of the Autumn Tibetan Plateau snow cover on the winter temperature over North America in the mid-1990s. *J. Geophys. Res.*, **124**, 10 321–10 343, https://doi.org/10.1029/2019JD030245.

Thomas W., and NOAA CDR Program (2012): NOAA Climate Data Record (CDR) of Northern Hemisphere (NH) Snow Cover Extent (SCE), Version 1.. NOAA National Centers for Environmental Information [Available online at https://doi.org/10.7289/V5N014G9].

Sardeshmukh, P. D., and B. J. Hoskins, 1988: The generation of global rotational flow by steady idealized tropical divergence. *J. Atmos. Sci.*, **45**, 1228–1251, https://doi.org/10.1175/1520-0469(1988)045<1228:TGOGRF>2.0.CO;2.

Schiemann, R., D. Lüthi, P. L. Vidale, and C. Schär, 2008: The precipitation climate of central Asia—Intercomparison of observational and numerical data sources in a remote semiarid region. *International Journal of Climatology*, **28**, 295–314, https://doi.org/10.1002/joc.1532.

Si, D., and Y. H. Ding, 2013: Decadal change in the correlation pattern between the tibetan plateau winter snow and the East Asian summer precipitation during 1979-2011. *J. Climate*, **26**, 7622–7634, https://doi.org/10.1175/JCLI-D-12-00587.1.

Siegfried, T., T. Bernauer, R. Guiennet, S. Sellars, A. W. Robertson, J. Mankin, P. Bauer-Gottwein, and A. Yakovlev, 2012: Will climate change exacerbate water stress in Central Asia? *Climate Change*, **112**, 881–899, https://doi.org/10.1007/s10584-011-0253-z.

Wang, Z. B., R. G. Wu, S. F. Chen, G. Huang, G. Liu, and L. H. Zhu, 2018a: Influence of Western Tibetan Plateau summer snow cover on East Asian summer rainfall. *J. Geophys. Res. Atmos.*, **123**, 2371–2386, https://doi.org/10.1002/2017JD028016.

Wang, Z. B., R. G. Wu, and G. Huang, 2018b: Low-frequency snow changes over the Tibetan Plateau. *International Journal of Climatology*, **38**, 949–963, https://doi.org/10.1002/joc.5221.

Wang, Z. B., R. G. Wu, P. Zhao, S.-L. Yao, and X. J. Jia, 2019: Formation of snow cover Anomalies Over the Tibetan Plateau in cold seasons. *J. Geophys. Res. Atmos.*, **124**, 4873–4890, https://doi.org/10.1029/2018JD029525.

Watanabe, M., 2004: Asian jet waveguide and a downstream extension of the North Atlantic Oscillation. *J. Climate*, **17**, 4674–4691, https://doi.org/10.1175/JCLI-3228.1.

Wu, Z. W., Z. H. Jiang, J. P. Li, S. S. Zhong, and L. J. Wang, 2012: Possible association of the western Tibetan Plateau snow cover with the decadal to interdecadal variations of northern China heatwave frequency. *Climate Dyn.*, **39**, 2393–2402, https://doi.org/10.1007/s00382-012-1439-4.

Wu, Z. W., X. X. Li, Y. J. Li, and Y. Li, 2016: Potential influence of arctic sea ice to the interannual variations of East Asian spring precipitation. *J. Climate*, **29**, 2797–2813, https://doi.org/10.1175/JCLI-D-15-0128.1.

Xiao, Z. X., and A. M. Duan, 2016: Impacts of Tibetan Plateau snow cover on the interannual variability of the East Asian summer monsoon. *J. Climate*, **29**, 8495–8514, https://doi.org/10.1175/JCLI-D-16-0029.1.

Yao, J. Q., and Y. N. Chen, 2015: Trend analysis of temperature and precipitation in the Syr Darya Basin in Central Asia. *Theor. Appl. Climatol.*, **120**, 521–531, https://doi.org/10.1007/s00704-014-1187-y.

You, Y. J., and X. J. Jia, 2018: Interannual variations and prediction of spring precipitation over China. *J. Climate*, **31**, 655–670, https://doi.org/10.1175/JCLI-D-17-0233.1.

Yuan, X. L., W. F. Wang, J. J. Cui, F. H. Meng, A. Kurban, and P. De Maeyer, 2017: Vegetation changes and land surface feedbacks drive shifts in local temperatures over Central Asia. *Scientific Reports*, **7**, 3287, https://doi.org/10.1038/s41598-017-03432-2.

Zhang, P., Z. W. Wu, J. P. Li, and Z. N. Xiao, 2020: Seasonal prediction of the northern and southern temperature modes of the East Asian winter monsoon: The importance of the Arctic sea ice. *Climate Dyn.*, **54**, 3583–3597, https://doi.org/10.1007/s00382-020-05182-w.

Zhang, Y. S., T. Li, and B. Wang, 2004: Decadal change of the spring snow depth over the Tibetan Plateau: The associated circulation and influence on the East Asian summer monsoon. *J. Climate*, **17**, 2780–2793, https://doi.org/10.1175/1520-0442(2004)017<2780:DCOTSS>2.0.CO;2.

Zhao, H. X., and G. W. K. Moore, 2006: Reduction in Himalayan snow accumulation and weakening of the trade winds over the Pacific since the 1840s. *Geophys. Res. Lett.*, **33**, L17709, https://doi.org/10.1029/2006GL027339.

Zhao, P., and L. X. Chen, 2001: Climatic features of atmospheric heat source/sink over the Qinghai-Xizang Plateau in 35 years and its relation to rainfall in China. *Sci. China, Ser. D Earth Sci.*, **44**, 858–864, https://doi.org/10.1007/BF02907098.

Zhao, P., Z. J. Zhou, and J. P. Liu, 2007: Variability of Tibetan spring snow and its associations with the hemispheric extratropical circulation and East Asian Summer Monsoon rainfall: An observational investigation. *J. Climate*, **20**, 3942–3955, https://doi.org/10.1175/JCLI4205.1.